JOURNAL OF APPLIED ELECTROCHEMISTRY **29** (1999) 1–6

Influence of silver on electrochemical and corrosion behaviours of Pb–Ca–Sn–Al grid alloys Part I: Potentiodynamic and potentiostatic studies

S. ZHONG, J. WANG, H. K. LIU, S. X. DOU

Institute for Materials Technology and Manufacturing, University of Wollongong, NSW 2522 Australia

M. SKYLLAS-KAZACOS

School of Chemical Engineering and Industrial Chemistry, University of New South Wales, NSW 2052, Australia

Received 9 September 1997; accepted in revised form 23 January 1998

The influence of silver, in the range of 0.02 wt% to 0.07 wt%, on the electrochemical and corrosion properties of Pb–Ca–Sn–Al grid alloy in sulphuric acid solutions at room temperature was investigated by potentiodynamic and potentiostatic methods. The introduction of Ag into a common grid alloy of Pb–Ca–Sn–Al confers some important features on the alloy. Potentiodynamic anodic polarisation measurements provided a qualitative overview of the activating, passivating and transpassivating processes which correspond to $Pb \rightarrow PbSO_4$, $PbSO_4 \rightarrow PbO_2$ reactions respectively. Cyclic voltammetric measurements provided information on the effect of Ag on the oxidation of $PbSO_4$ to PbO_2. The addition of Ag refined the grains and enhanced the passivation of the electrode and its corrosion resistance. A decrease in the oxygen evolution overpotential and an increase in the hydrogen evolution overpotential with the additions of Ag were also observed during the experiments.

Keywords: *lead acid battery*, *grid alloy*, *silver*, *electrochemical behaviour*, *corrosion behaviour*

1. Introduction

The primary properties of interest in grid alloys for lead–acid batteries are the mechanical strength and the corrosion resistance, as well as the compatibility with the active materials (adherence), castibility and electrochemical properties. Pb–Ca alloys were proposed as grid alloys as early as the 1935 [1], but extensive research has been reported since the 1970s [2]. These alloys, due to the high H_2 and O_2 overpotentials, are commercially used today in the new generation of valve-regulated lead–acid batteries (VRLABs). Although the tensile strength of cast Pb–Ca and Pb–Sb alloys are similar, the creep strength of cast Pb–Ca alloys is much lower than that of their antimony counterparts. Pb–Ca alloys have a tendency for nonuniform corrosion due to preferred grain boundary attack and this leads to a swelling effect in the material due to growth of intergranular corrosion products which gives rise to an apparent 'growth' of positive grids in service. Since the creep strength is closely correlated to the grid growth, therefore, Pb–Ca type alloys suffer more severe positive-grid growth in service than Pb–Sb alloys [3].

There has been a series of studies that have involved the improvement of the mechanical properties (especially in the creep strength) and the corrosion stability of Pb–Ca alloys by further addition of alloying elements [4]. Ag is one of the most attractive of these grid alloying elements, with claims that it can improve both the corrosion stability and the creep strength even at a comparatively low concentration of 0.01 to 0.1 wt% [5]. Various mechanisms of alloying Ag to Pb and Pb alloys have been proposed which consider either electrochemical properties or microstructure. The favourable effects of Ag addition have been attributed to (i) dispersing the structure of the alloys and increasing the compactness of the PbO_2 film (the formation of a high-dispersion intermetallide causes an increase in the corrosion resistance of the alloy [6]), (ii) lowering of the O_2 overpotential at the positive electrode, therefore, reducing the corrosion rate under constant current overcharge conditions [7] and (iii) catalytic activity in decomposing the oxidizing persulphate ion, thus indirectly preventing the formation of more PbO_4 from $PbSO_4$ [8]. Although extensive research was performed on Pb and Pb–Sb alloy system, very little relates to the effect of Ag on the common grids of Pb–Ca–Sn(–Al). The effect of Ag on the mechanical properties of the alloys was previously reported [9]. The present study aims at elucidating the influence of alloying Ag on the electrochemical and corrosion properties of a common Pb–Ca–Sn–Al grid alloy. To this end, potentiodynamic and potentiostatic measurements were performed; the effect of Ag on alloy microstructure and

on the H_2 and O_2 evolution reactions are reported in this paper.

2. Experimental details

The preparation of working electrodes, the electrode surface treatment and the experimental set-up were described in detail previously [10]. A nominal alloy composition of Pb–0.09 wt% Ca–0.5 wt% Sn–0.02 wt% Al, was chosen as the base alloy. Ag (Aldrich Chem. Co. 99.99%) was added to the molten alloy at about 400 °C under argon protection. The compositions of four group electrodes analysed by ICP (inductively coupled plasma spectroscopy) are listed in Table 1. A three-compartment electrolytic cell separated by glass frits was used in the experiments. The reference electrode was Hg/Hg_2SO_4 (K_2SO_4 saturated solution) which terminated in a Luggin capillary and all potentials are referred to this scale. The counter electrode was a pure lead sheet (99.99%). Electrolytes used in the experiments were 0.5 M and 1.28 sp.gr. H_2SO_4 solutions, prepared from 98 wt% at 25 °C H_2SO_4 (Univar A.R.) with double-distilled water. The electrolytes used were deaerated with high purity nitrogen for 1 h before immersion of the test electrode in the solution. A constant temperature of 20 °C was provided by a thermostat controlled water bath (Julabo refrigerated, circulated mode F10-MH, Germany). Potentiodynamic anodic polarization and cyclic voltammetric measurements were performed by a scanning potentiostat (model 362, EG&G Princeton Applied Research), which was connected via a MachLab/8 interface (Analog Digital Instruments, AD Instruments Pty Ltd) to a Macintosh computer supported by the Chart v.3.5 software. The anodic polarisation measurements were performed in accordance with standard ASTM G5-87.

Cyclic voltammetric measurements were performed after the working electrodes were 'initiated' up to +2000 mV in the first cycle [11] in the 1.28 sp.gr. H_2SO_4 solution. Hydrogen evolution rates were measured in the 1.28 sp.gr. H_2SO_4 solution by slow linear sweep voltammetry (LSV). Each working electrode was held initially at a potential of −1.3 V for 30 min. This treatment is used to reduce any surface oxide on the working electrode surface. The working electrode potential was then scanned from −1.3 to −1.8 V at a rate of 0.1 mV s^{-1} and the current, representing the hydrogen evolution rate, was recorded. The hydrogen overpotential measurements were also performed under steady-state conditions at constant current densities of 1.6 mA cm^{-2} and 4.8 mA cm^{-2}. Since the oxygen evolution on the electrode surface is affected by the quantity of lead dioxide on the electrode surface, oxygen evolution measurements were approached by a step-potentiostatic procedure accompanied by gas collection, the method has been previously described [10]. Each electrode was freshly polished and was held at the given potential until the current became constant. The constant current was recorded and, then, the gas evolved was collected during a certain period.

The oxygen evolution current density, i_{O_2} (A cm^{-2}) according to Faraday's law, was calculated by [12]:

$$i_{O_2} = \frac{4F(P_{atm} - P_w)V}{RTAt} \quad (1)$$

where P_{atm} is atmospheric pressure and P_w the vapour pressure at the absolute temperature T. F is the Faraday constant, V the gas volume measured by the 'soap-bubble method' in m^3, R the gas constant (= 8.314 J mol^{-1} K^{-1}), t the electrolysis time in seconds and A is the electrode area in cm^2. The same procedure was repeated at each given potential.

Table 1. Alloy composition by ICP analysis (wt %)

Electrode	*Alloy composition wt % determined by ICP*			
	Ca	*Sn*	*Al*	*Ag*
1	0.105	0.538	0.018	–
2	0.106	0.530	0.012	0.02
3	0.102	0.561	0.010	0.053
4	0.110	0.529	0.012	0.071

3. Results and discussion

3.1. *Potentiodynamic anodic polarization plots*

Potentiodynamic anodic polarisation plots at 20 °C in 0.5 m H_2SO_4 solution are presented in Fig. 1. These plots provide a qualitative overview of the activating, passivating and transpassivating processes which correspond to the reactions: $Pb \rightarrow PbSO_4$ and $PbSO_4 \rightarrow PbO_2$. Region A in Fig. 1 is the active region in which the specimen electrode corrodes as the applied potential is made more positive and corresponds to $Pb \rightarrow PbSO_4$. At B further increase in the current density ceases with the onset of passivation. In region C the current decreases rapidly as the passivating film forms on the specimen. Increasing in the applied potential causes the passivating film to break down in region D, the transpassive region, corresponding to the reaction: $PbSO_4 \rightarrow PbO_2$. With

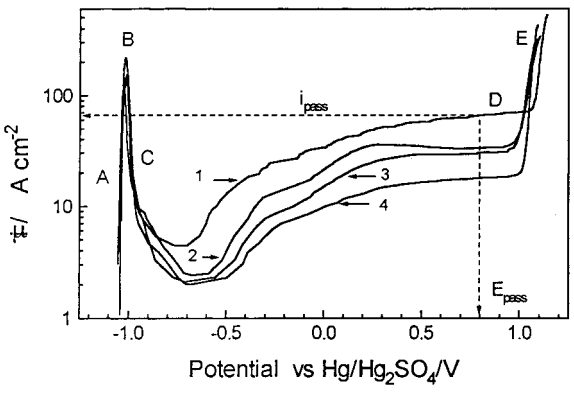

Fig. 1. Anodic polarizaion plots for different Ag additions at 20 °C in 0.5 M H_2SO_4. Sweep rate 0.1 mV s^{-1}. Key: (1) Pb–Ca–Sn–Al; (2) +0.02 Ag; (3) +0.05 Ag; (4) +0.07 Ag.

further increase in the potential in region E, O_2 begins to evolve. Data from these experiments at a given passive potential E_{pass}, are presented in Table 2, where i_{pass} is the passive current density at the passive potential E_{pass} and E_{55} is the corrosion potential at open-circuit after immersion, for 55 min.

To understand the effect of Ag on the anodic polarization plots in Fig. 1, the plot of the electrode without Ag addition should be compared with those of the Ag electrodes in Fig. 1. The passive layer has been demonstrated to be a two-layer structure, that is, $Pb/PbO_x/PbSO_4$ [13]. The stability of the passive layer, as evaluated by the passive current density, increases proportionally with the Ag addition. It can be seen that the anodic plots in the oxygen evolution region, E, with the increase in the Ag concentration in the alloy, shift in the negative potential direction (about 20 mV) and the oxygen overpotential drops. These suggested that the addition of Ag decreases the oxygen overpotential, modifies the two- layer structure (increases the compactness of PbO_x film) and make the passive layer more stable which corresponds to the lower passive current densities shown in Fig. 1 and Table 2.

3.2. *Cyclic voltammetric measurements*

The anodic corrosion of the Pb electrode to PbO_2 is due to oxygen penetrating across the anodic layer. The different electrode systems formed on the basis of the different structures of the anodic layer were disclosed by Pavlov *et al.* [14] and D. Pavlov *et al.* [15], while the membrane properties of the $PbSO_4$ layer were reported in [16, 17]. The structure and composition of the anodic layer all are determined by the electrode potential. From −400 to +950 mV vs Hg/Hg_2SO_4, the anodic layer shows the following structure: Pb/PbO layer/$PbSO_4$ membrane/H_2SO_4 solution. The $PbSO_4$ crystals form a membrane and a dense layer of *tet*-PbO is situated between the $PbSO_4$ layer and the metal.

Above +950 mV, the anodic layer contains α-PbO_2, β-PbO_2 and *tet*-PbO.

The Pb^{2+} ions formed as a result of the dissolution of $PbSO_4$ crystals are oxidized to PbO_2, according to

$$Pb^{2+} + 2\ H_2O \rightarrow PbO_2 + 4\ H^+ + 2\ e^- \qquad (2)$$

PbO and PbO_x found in the pores of the $PbSO_4$ membrane are oxidized through solid-state reactions to α-PbO_2. When α-PbO_2 is contact with H_2SO_4, the Pb^{2+} ions formed by the dissolution of $PbSO_4$ are oxidized according to Reaction (2) yielding β-PbO_2, because the medium is acidic [13].

Linear sweep voltammetry is one of the most popular methods used to study the anodic layer oxidation of $PbSO_4$ to PbO_2. It has been reported [18] that a 'stabilized electrode' can be obtained by cycling to a constant response between the limits +400 and +1520 mV in linear sweep experiments. Although the corrosion stability of a given metal on formation of an anodic layer is determined generally through the weight losses (under a constant anodic potential), it can be used to simulate the battery under the float charging condition but not under the cycling condition. The anodic peak current density, i_p, does not connect to the anodic corrosion stability, however, the constant response curves of the maximum peak current values, i_{pmax}, can be used to compare the stability of the anodic layer of different electrodes under a cycling condition, which is a close simulation of the condition when a battery under cycling charge-discharge processes.

In the present experiment, the potential of the electrode was swept up to +2000 mV in the first cycle and then cycled between +500 and +1600 mV. The rate of attainment of constant response is studied by following changes in the peak current values (i_p) as the electrode is cycled. The peak current density value, i_p, against cycle number is plotted in Fig. 2 which provides information of the effect of Ag addition on the oxidation of $PbSO_4$ (*tet*-PbO) to PbO_2. The results suggest that the Ag additions vary the kinetic barrier for the formation of PbO_2 from $PbSO_4$ and inhibit the oxidation of $PbSO_4$ to PbO_2.

3.3. *Hydrogen evolution reaction rate and overpotential*

The rate of the hydrogen evolution reaction on different electrodes was measured by slow linear sweep experiments (sweep rate 0.1 mV s^{-1} in 1.28 sp.gr. H_2SO_4 solution) and the results are presented in Fig. 3.

Table 2. Data from potentiodynamic anodic polarization plots in Fig. 1

Electrode	E_{55}/V	E_{pass}/V	$i_{pass}/\mu A\ cm^{-2}$
1	−1.022	0.8	65.81
2	−1.027	0.8	33.24
3	−1.022	0.8	30.06
4	−1.021	0.8	18.12

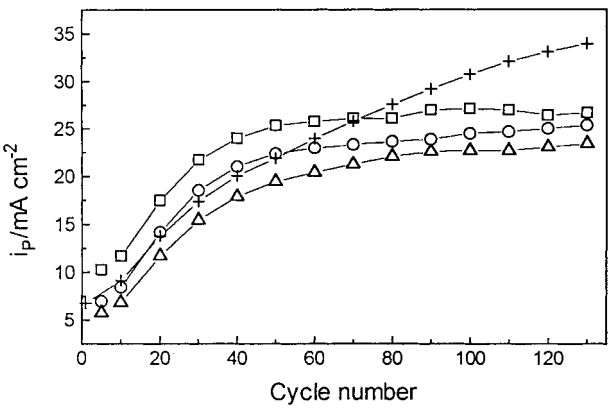

Fig. 2. Increase in PbO_2 peak current density values (i_p) against cycle number for different Ag additions. Electrode are cycled between +500 mV and +1600 mV. Sweep rate 2 mV s^{-1}. Key: (+) Pb–Ca–Sn–Al; (□) +0.02 Ag; (◯) +0.05 Ag; (Δ) +0.07 Ag.

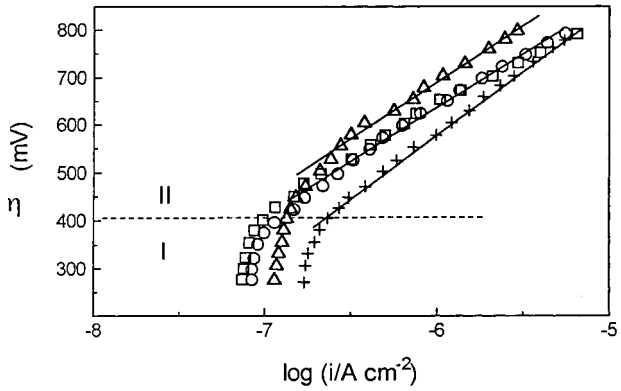

Fig. 3. Tafel plots corresponding to hydrogen evolution on electrodes with different Ag content in 1.28 sp. gr. H_2SO_4. Sweep rate 0.1 mV s^{-1}, $\eta = E - E_0$. Key: (+) Pb–Ca–Sn–Al; (□) +0.02 Ag; (○) +0.05 Ag; (Δ) +0.07 Ag.

The kinetics of hydrogen evolution reaction can be expressed by the Tafel equation. The potential/pH diagram [19] of $Pb/H_2O/H_2SO_4$ system shows that a H_2/H^+ equilibrium is established upon the Pb surface in H_2SO_4 solution:

$$2\ H^+ + 2\ e^- = H_2 \tag{3}$$

Since the equilibrium potential of H_2/H^+ cannot be obtained experimentally, it can be calculated theoretically from the Nernst equation. The calculated value of E_{eq}, is −578.4 mV vs Hg/Hg_2SO_4 at the electrolyte under the experimental temperature [20].

It should be pointed out that in addition to the hydrogen evolution reaction (3), lead becomes thermodynamically unstable at pH values less than 6. The following reactions also take place on the Pb electrode when it is immersed in H_2SO_4 solution:

$$Pb + SO_4^{2-} = PbSO_4 + 2\ e^- \tag{4}$$

$$\phi(Pb/Pb^{2+}) = \phi^0(Pb/Pb^{2+}) - \frac{RT}{2F}\ln\ a_{SO_4^{2-}} \tag{5}$$

$$Pb + HSO_4^- = PbSO_4 + H^+ + 2\ e^- \tag{6}$$

$$\phi(Pb/Pb^{2+}) = \phi^0(Pb/Pb^{2+}) - \frac{RT}{2F}\ln\ \frac{a_{H^+}}{a_{HSO_4^-}} \tag{7}$$

It can be seen from potential/pH diagram that the equilibrium potential of H_2/H^+ is more positive than that of $Pb/PbSO_4$ (about 0.3 V). Therefore, in this case no true equilibrium occurs for hydrogen evolution reaction even on open circuit at the rest potential. The rest potential is a mixed potential in which the anodic and cathodic current are equal. So that the hydrogen equilibrium potential could be a problem in electro-kinetics in such a 'multiple electrode system' for it always accompanies the equilibrium potential of the process: $Pb + SO_4^{2-} = PbSO_4 + 2\,e^-$ (or other reaction). For the consistent application of thermodynamics in which the reversible equilibrium is obtained normally at vanishing current density, the difference from the overall current–free potential E_0 (a zero-current potential or a steady-state potential at open circuit) has been used frequently as the reference potential for the measurement of the hydrogen overpotential [10, 12, 20, 21], rather than the E_{eq} calculated from the Nernst equation, that is,

$$\eta = E - E_0 \tag{8}$$

The Tafel plots with η referred to E_0 are presented in Fig. 3.

Although the Tafel slopes, b, obtained with reference to E_{eq} and E_0 are the same, the corresponding 'overpotential' values and the 'exchange current density' are different. This should be kept in mind when comparing experimental data with different reference potentials (E_{eq} or E_0). Although i_0 calculated relative to E_0 is not the true i_0 for the hydrogen evolution reaction it is useful for the purpose of comparing the effect of the additive on the kinetics of the hydrogen reaction on the lead alloys.

The Tafel slopes present two different linear regions, region I at low overpotentials and region II at high overpotentials. This may be attributed to the fact that under lower overpotentials, only a small quantity of hydrogen (H_2) is produced and adsorbed on the electrode surface. This cannot readily escape from the electrode surface due to the liquid surface tension, so the 'effective active area' for the hydrogen evolution reaction on the electrode surface is reduced. Therefore, the increase in the hydrogen evolution current as the electrode potential moves in the more negative direction is balanced by a decrease in the effective active surface area. The data in region I do not accurately represent the kinetics of the hydrogen evolution reaction. However, the situation is different at high overpotentials in region II. Here the electrode surface is continuously renewed by the hydrogen gas which is produced vigorously so there is no blockage of the electrode. Only these data are presented in Table 3. A similar phenomenon has been reported by N. Papageorgiou *et al.* [22] and Lam *et al.* [12]. This phenomenon has also been explained in terms of the effect of the adsorption of anions on the electrode surface under different electrode potentials. The adsorbed anions depend on the potential in the double layer, and they can alter the distribution of the surface charge, which in turn will change the surface H^+ concentration and hence the reaction rate and the corresponding Tafel slope. Carr *et al.* [23] have reported that the quantity of adsorbed SO_4^{2-} ions on the Pb electrode surface decreases at high cathodic potentials. When the potential is reduced, the re-adsorption of SO_4^{2-} ions proceeds at a lower rate.

Table 3. Tafel parameters for hydrogen evolution reaction on electrodes with different Ag additions at region II

Electrode wt % Ag	*Region II*	
	b/V	$log(i_0/A\ cm^{-2})$
–	−0.20	−8.27
0.02	−0.19	−9.11
0.05	−0.19	−8.96
0.07	−0.20	−9.18

The Tafel slope values in Table 3 indicate that electrodes with different Ag additions show the same mechanism of hydrogen evolution. The small difference in the exchange-current density, i_0, for the different electrodes makes it difficult to define the effect of Ag addition on the hydrogen evolution reaction. To clarify the effect of Ag on the hydrogen overpotential, a controlled-current experiment was performed. Hydrogen overpotentials were thus obtained under 'steady-state conditions' at constant current densities of 1.6 mA cm^{-2} and 4.8 mA cm^{-2}, and plotted in Fig. 4. These results clearly show a trend of increasing the hydrogen overpotential with the addition of Ag. The effect of Ag on the hydrogen overpotential may be attributed to the variations in the alloy microstructure [24] due to the addition of Ag and indicates that 'the effective active area' of hydrogen evolution on the electrode surface could be decreased, or the 'absorption of anions' on the electrode surface could be changed. This may alter the electrocatalytic properties of the electrode surface and affect the hydrogen-to-metal bonding energy, thus, influencing the rate of hydrogen evolution.

3.4. *Oxygen evolution reaction rates*

When a Pb electrode is immersed in H_2SO_4 solution and polarized anodically in the PbO_2 potential region the $Pb/PbO_2/PbSO_4/H_2SO_4/H_2O/O_2$ electrode system is established [25]. According to the potential/pH diagram [17], two redox reactions occur on the electrode: one is the evolution or reduction of oxygen, and the other the oxidation of $PbSO_4$ or reduction of PbO_2. The oxygen evolution reaction occurs at the anodic layer–solution interface and the oxygen evolution rate is affected by the quantity of PbO_2 on the electrode surface.

In the present experiment the oxygen evolution rate was studied using the gas collection [12] and 'partial steady-state current' methods [26], and the results are presented in Fig. 5. These plots show that Ag enhances the oxygen evolution and the enhancement is proportional to the Ag content. The oxygen evolution efficiency, σ, is calculated by the ratio during charging,

$$\sigma = Q_{O_2}/Q_t \tag{9}$$

where $Q_{O_2} = j_{O_2} \times t$, is the charge in coulombs calculated from the gas volume collected according to Equation 1; Q_t is the total charge in coulombs recorded during the charging process.

The data are presented in Table 4. These results show that although the oxygen is evolved at a steady-state (i.e., the current reaches a constant value at a given potential), the proportion of current going into gas production is low at low anodic potentials, and high at high anodic potentials. It is known that the current density recorded during the gassing measurement, i_{total}, is the sum of the anodic corrosion current density, i_{corr}, and the oxygen evolution current density, i_{O_2} (i.e., $i_{total} = i_{corr} + i_{O_2}$) so that $\sigma = i_{O_2}/(i_{O_2} + i_{corr})$. The results in Fig. 6 and Table 4 thus indicate when the anodic potential is kept at a constant value in the oxygen evolution region, the introduction of silver in the alloy accelerates the oxygen evolution, but the opposite effect is observed for the anodic corrosion of the alloy. In other words, under a given current density charge condition, the anodic corrosion current density, i_{corr}, will be lower on the electrodes with Ag addition than on the electrodes without Ag. Thus high corrosion resistance alloys can be obtained with Ag additions. This result is consistent with the results from anodic polarisation and cyclic voltammetric measurements.

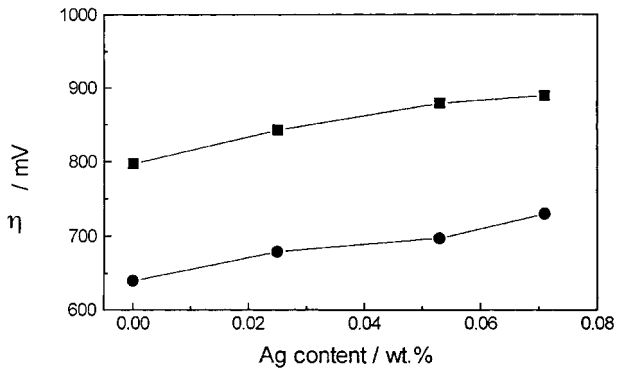

Fig. 4. Hydrogen overpotentials on electrodes with different Ag constant under constant current conditions, at 20 °C in 1.28 sp.gr. H_2SO_4, $\eta = E - E_0$. Key: (●) 1.6 mA cm^{-2}; (■) 4.8 mA cm^{-2}.

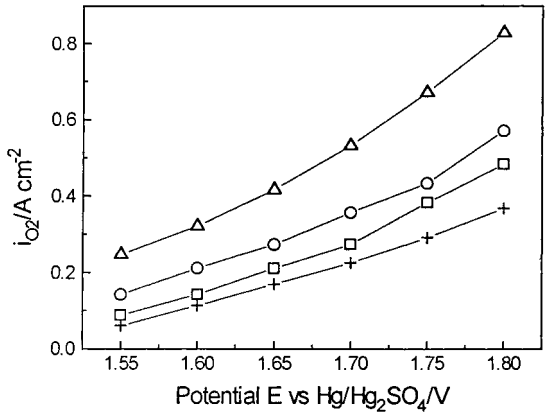

Fig. 5. Oxygen evolution on different Ag electrodes in 1.28 sp. gr. H_2SO_4 at 20 °C. Key: (+) Pb–Ca–Sn–Al; (Δ) +0.07 Ag; (◯) +0.05 Ag; (□) 0.02 Ag.

Table 4. Oxygen evolution efficiency (%) at different potentials

Potentials vs $Hg/Hg_2SO_4/V$	*wt % Ag*			
	0	*0.02*	*0.05*	*0.07*
1.55	84.3	88.2	93.1	96.2
1.60	87.6	91.0	94.4	96.6
1.65	90.3	92.6	94.7	96.8
1.70	92.5	93.7	95.9	97.2
1.75	93.6	95.4	96.3	97.5
1.80	94.9	96.3	97.1	98.1

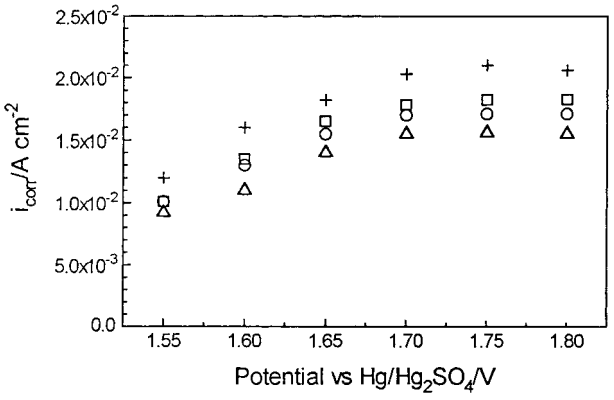

Fig. 6. Corrosion current density of electrodes with different Ag content calculated from Fig. 5 and Table 4. Key: (+) Pb–Ca–Sn–Al; (□) +0.02 Ag; (◯) +0.05 Ag; (Δ) 0.07 Ag.

4. Conclusions

(i) The incorporation of Ag in a common Pb–Ca–Sn–Al alloy, was found in the present study to decrease the passive current density, enhance the stability of the oxide passive film and increase the anodic corrosion resistance.

(ii) The gassing properties of the Pb–Ca–Sn–Al alloy used in the present study show that the addition of Ag to the common Pb–Ca–Sn–Al alloy inhibits hydrogen evolution rates and increases hydrogen overpotential, enhances the oxygen evolution rates and decreases oxygen overpotential. These properties are considered to provide a beneficial effect from the view of gas recombination in VRLA batteries.

References

[1] B. U. Thomas, F. T. Forster and H. E. Harring, *Trans. Am. Electrochem. Soc.* **92** (1947) 313.
[2] N. E. Bagshaw, *J. Power Sources* **33** (1991) 3.
[3] J. Perkings, J. L. Pokorny and M. T. Cole, A review of materials and mechanisms which affect the performance of lead/acid storage batteries. Naval Postgraduate School, California (Oct. 1976).
[4] N. E. Bagshaw, *J. Power Sources* **53** (1995) 25.
[5] *US Patent 5 298 450* (1994).
[6] M. A. Dasoyan and I. A. Aguf, 'Current Theory of Lead Acid Batteries', ILZRO Inc. New York (1979).
[7] D. Pavlov and T. Rogachev, *Electrochim. Acta.* **31** (1986) 241.
[8] J. J. Lander, *J. Electrochemical Soc.* **105** (1958) 289.
[9] S. Zhong, H. K. Liu, S. X. Dou and M. Skyllas-Kazacos, *J. Power Sources* **59** (1996) 123.
[10] S. Zhong, J. Wang, H. K. Liu, S. X. Dou and M. Skyllas-Kazacos, *ibid.* **66** (1997) 105.
[11] N. A. Hampson and S. Kelly, *J. Appl. Electrochem.* **11** (1981) 751.
[12] L. T. Lam, R. De Marco, J. D. Douglas, R. Pillig and D. A. J. Rand, *J. Power Sources* **48** (1994) 219.
[13] D. Pavlov and Z. Dinev, *J. Electrochem. Soc.* **127** (1980) 855.
[14] D. Pavlov, C. N. Poulieff, E. Klaja and N. Iordanov, *J. Electrochem. Soc.* **116** (1969) 316.
[15] D. Pavlov and N. Iordanov, *ibid.* **117** (1970) 1103.
[16] D. Pavlov and R. Povlova, *Electrochim. Acta.* **15** (1970) 1483.
[17] P. Ruetschi, *J. Electrochem. Soc.* **120** (1973) 331.
[18] S. Kelly and N. A. Hampson, *in* 'Research and Development in Non-Mechanical Electrical Power Sources (edited by J. Thompson). Proceedings of the 12th International Power Sources Symposium (1980) *Power Sources* **8** (1981) 535.
[19] S. C. Barnes and R. T. Mathieson, *in* 'Batteries 2' (edited by D. H. Collins), Pegamon Press, Oxford (1965).
[20] H. Bode, 'Lead/Acid Batteries' (translated by R. J. Brodd and K. V. Koraesch), a Wiley-Interscience/J. Wiley & Sons (1977), p. 88.
[21] P. Ruetschi, J. B. Ockerman and R. Amlie, *J. Electrochem. Soc.* **107** (1960) 325.
[22] N. Papageorgiou and M. Skyllas-Kazacos, *Electrochim. Acta* **37** (1992) 269.
[23] J. P. Carr, N. A. Hampson, S. N. Holley and R. Taylor, *J. Electroanol. chem.* **32** (1971) 345.
[24] S. Zhong, J. Wang, H. K. Liu, S. X. Dou and M. Skyllas-Kazacos, to be submitted.
[25] D. Pavlov, 'Power Sources for Electric Vehicles' (edited by B. D. McNicol and D. A. J. Rand), Elsevier, Amsterdam (1984), p. 167.
[26] D. Pavlov, *Electrochim. Acta* **31** (1986) 241.